Journal of Physics:
Conference Series

PAPER • **OPEN ACCESS**

The 4K difference due to radiative trapping: a numerical study of overheating in urban canyon dwellings

To cite this article: Valentin Lahaye *et al* 2025 *J. Phys.: Conf. Ser.* **3140** 082003

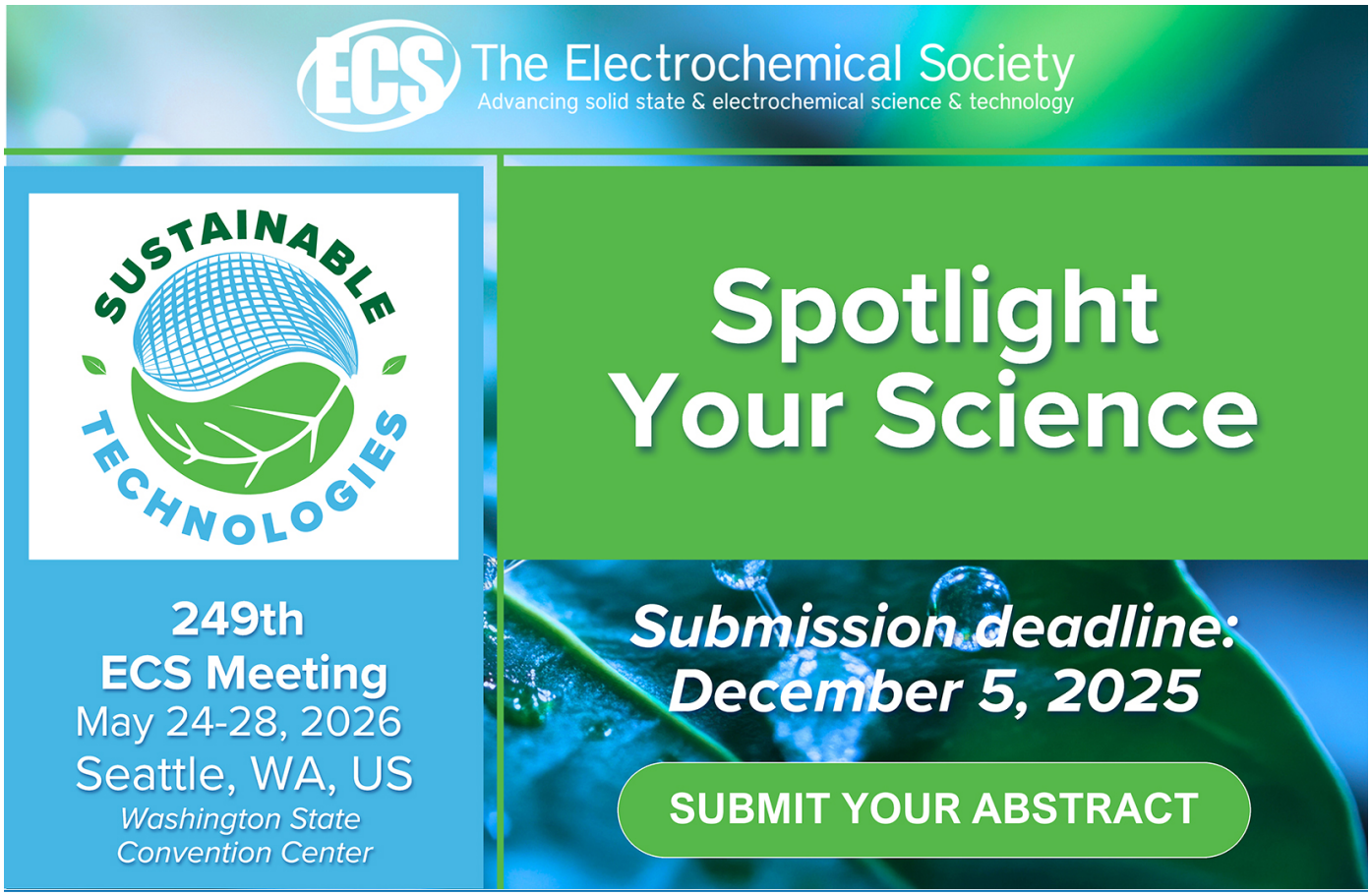

Journal of Physics: Conference Series **3140** (2025) 082003 doi:10.1088/1742-6596/3140/8/082003

The 4K difference due to radiative trapping: a numerical study of overheating in urban canyon dwellings.

Valentin Lahaye[1], Marion Bonhomme[1], Claire Oms[1], Nicolas Duport[2], Stéphane Ginestet[1].

[1] LMDC, Université de Toulouse, INSA, UPS, Toulouse, France

[2] B2R, UniLaSalle, Amiens, France

lahaye@insa-toulouse.fr

Abstract. Improving our understanding of thermal interactions between urban buildings is a major challenge regarding future climate projections. In this paper, we quantify the influence of radiative trapping on indoor thermal comfort into dwellings located in an urban canyon during a summer heatwave. A numerical urban model based on the finite element method (FEM) coupled to a radiosity method is used to simulate a Mediterranean city building. The complete thermal problem, including conduction, convection, and radiation, is solved in a transient regime using meteorological data representative of heatwave conditions. Physiological Equivalent Temperature (PET) indicator is used to assess indoor comfort, accounting for radiation exposure. The results show that longwave radiative trapping leads to a sustained increase in indoor PET of approximately 4K, whereas the influence of shortwave varies by ±1K.

1. Introduction and context

The risk of overheating in European cities is a growing concern in the context of climate disruption, which is characterized by more frequent and intense heat wave [1]. The urban heat island phenomenon is further exacerbated in highly urbanized city centers, where the radiation trapping between buildings leads to an increase in local temperatures [2]. However, currents Urban Building Energy Modelling (UBEM) have limitations to represent radiative interactions in urban environment [3]. The exchange of longwave radiation between buildings and the consideration of reflected solar radiation in urban canyons are mostly simplified, which is a barrier for the accuracy of simulations for indoor thermal comfort in city center. In this paper, we propose to evaluate the increasing of interior temperature during a heatwave by solving urban thermal simulations with a finite element method coupled by a radiosity method developed specifically for the study of radiation in urban environments [4], [5]. It permits highly detailed radiative calculations at the scale of the building and the street, by using complete urban scene mesh including the sky [6].

Three simulations are compared. The first one represents the building in its real environment and serves as a basis for comparison. The second uses the same shortwave irradiances as the first one but considers an unobstructed view for longwave radiation calculation. The third still considers an unobstructed view for the longwave but also consider complete shortwave absorption from the nearly building, which summed up to not considering any inter-reflection in the street. These two variants respectively quantify the influence of both longwave and shortwave radiative trapping.

2. Description of the methodology and the case study

The case study is a neoclassical building located on the street Paul Riquet in downtown Toulouse, France. The process for urban thermal calculations is detailed below in **figure 1.**

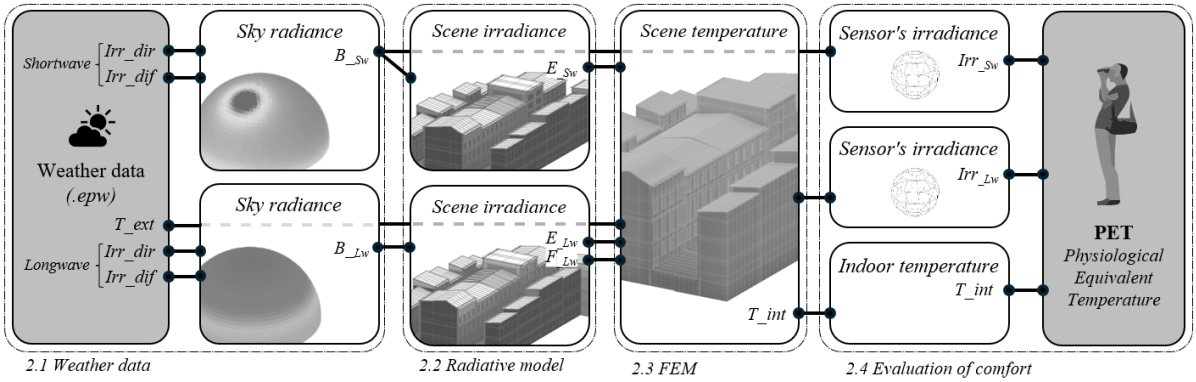

Figure 1: Schematic representation of the simulation process

2.1. Weather data

Toulouse EnergyPlus weather file [7] is used to generate a meteorological data representing a heatwave of magnitude 6 based on the forecasting radiative forcing [8]. This data is integrated into the model by decomposing the sky into 2000 tiles of equivalent solid angles [9], where the radiances are calculated from the distributions of Perez for short waves [10], and Martin and Berdahl for long waves [11].

2.2. Radiative model (from sky to the scene)

The calculation of radiation received by the scene from the sky is processed using a radiosity method based on the Embree ray-tracing algorithm [6]. This method presents the uses of extended view factor calculations, which consider many diffuse and specular reflections / transmissions (either perfectly diffused or perfectly specular), to calculate separately for shortwave and longwave. This approach is particularly suited in our urban case study where a maximum number of 20 reflections has been set for the calculation of view factors, regarding radiation properties of the materials detailed in below **(figure 2)**. τ_r is the specular transparency, τ_d is the diffuse transparency, ρ_r is the direct reflectance, ρ_d is the diffuse reflectance, α is the absorptivity, and ε the emissivity.

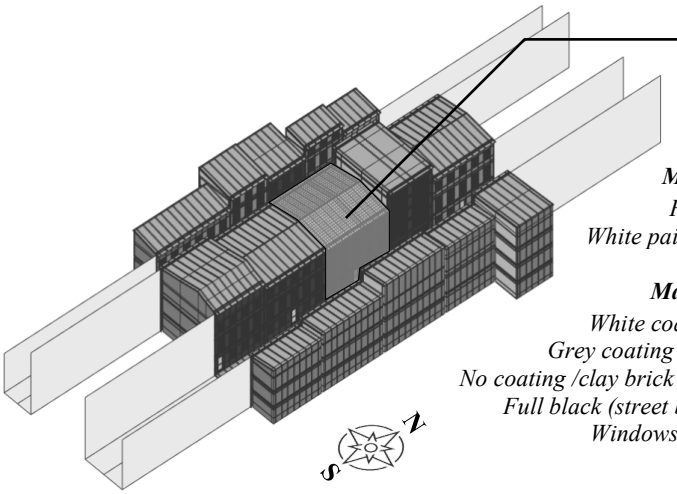

	Shortwave					Longwave
Materials (indoor)	τ_r	τ_d	ρ_r	ρ_d	α	ε
Floor tiles (white)	*0*	*0*	*0*	*0.80*	*0.20*	*0.90*
White paint (wall / ceiling)	*0*	*0*	*0*	*0.85*	*0.15*	*0.90*
Materials (outdoor)	τ_r	τ_d	ρ_r	ρ_d	α	ε
White coating (case study)	*0*	*0*	*0*	*0.70*	*0.30*	*0.90*
Grey coating (street buildings)	*0*	*0*	*0*	*0.40*	*0.60*	*0.90*
No coating /clay brick (street buildings)	*0*	*0*	*0*	*0.20*	*0.80*	*0.90*
Full black (street buildings, case 3)	*0*	*0*	*0*	*0*	*1*	*0.90*
Windows (double-glazing)	*0.80*	*0*	*0.10*	*0*	*0.10*	*0.90*
Street extension	*0*	*0*	*0*	*0*	*1*	*0.90*
Pavement	*0*	*0*	*0*	*0.10*	*0.90*	*0.90*
Clay roof tiles	*0*	*0*	*0*	*0.15*	*0.85*	*0.90*

Figure 2: Radiative properties of the building studied and its environment

Then, equation (1) gives the flux E_i [W.m^{-2}] received per unit area on faces i. The parameter F_{ij} is the view factor between faces i and j, and B_j [W.m^{-2}] is the radiosity of the face j.

$$E_i = \sum_{i=1}^{N} F_{ij} * B_j \quad (1)$$

At this step, the irradiances are calculated only from the sky radiosity. A schematic representation of view factors used as boundary conditions for the complete radiation calculation considered for the 3 simulations is provided below **(figure 3).**

The first case represents the real thermal environment of the street with reflections considered for both shorts-wave and long-wave. The second case considers longwave view factors calculated as an open filed for the building studied. By comparison with the initial model, the results illustrate the influence of longwave radiative trapping from nearby buildings. For the third case, view factors are calculated as the second one, and in addition, the solar reflectance of nearby buildings is equal to 0. Thus, the shortwave radiation calculation does not take account of inter-reflections into the street. By comparison with the second case, the results illustrate the influence of shortwave radiative trapping from nearby buildings.

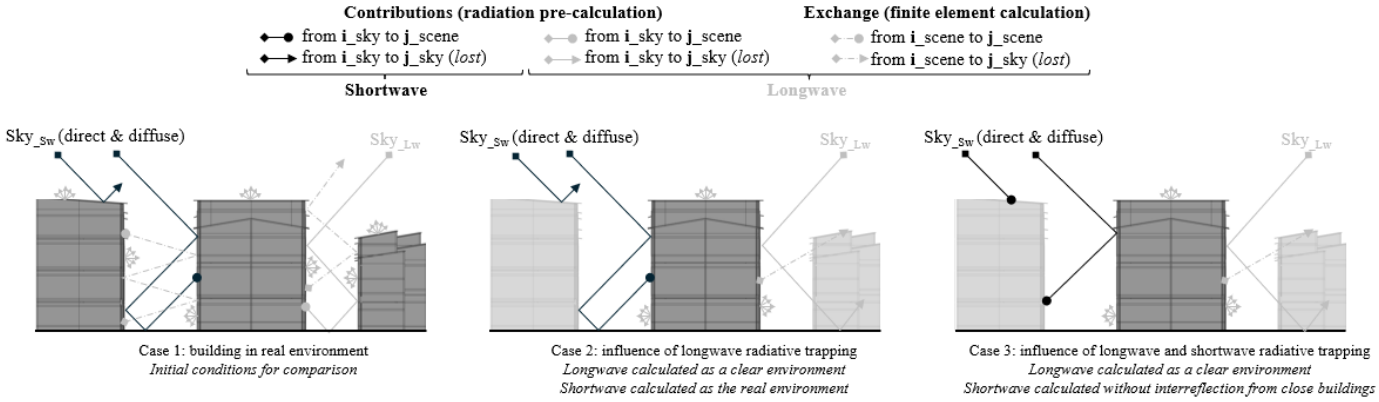

Figure 3: schematic representation of the view factor calculation (example of 3 reflections) on the three cases

2.3. Finite Elements Method (FEM)

The complete thermal problem (conduction, convection, radiation) is solved with the finite element method by using **Cast3m**, an opensource software developed by the CEA [12]. A modified version applied to integrate the radiative calculation of the pre-processed view factor is used [4].

To define the temperature field which will serve as initial conditions for the transient state calculation, the first step is solved in steady state. The following sections detail the calculation assumption for conduction, convection, and radiation, for both steady and transient states.

2.3.1. Conduction

Heat transfer by conduction is solved from the characteristics of the materials as thermal conductivity, density, and specific heat. Boundary conditions are imposed by convective and radiative flux on faces. Each building is constructed procedurally with a conformal mesh of maximum 0.5m for the study building, and 5.0m for the rest of the urban scene. To model the conductive transfer between two buildings, we use the method of "mesh gluing" [13].

However, the faces at the ends of the model are considered adiabatic (they do not exchange heat with the outside by conduction or radiation). In addition, a constant temperature of 15°C is set at ground level at a depth of 2.0 m.

Otherwise, all buildings are described according to the thermal properties as shown below (**figure.4**).

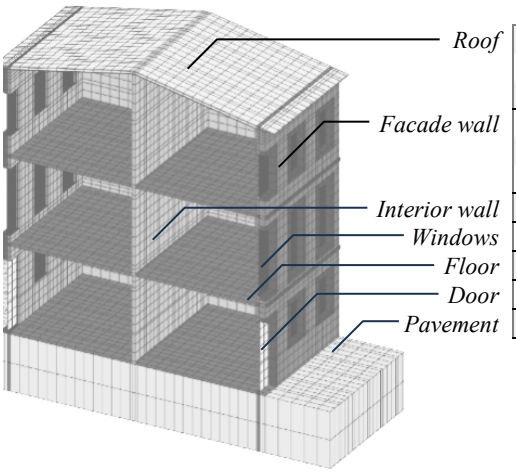

Materials	th [m]	λ [W.m^{-1}.K^{-1}]	ρ [kg.m^{-3}]	cp [J.kg^{-1}.K^{-1}]
Clay roof tiles	0.02	1.0	800	1700
Insulation	0.20	0.032	840	29
Plasterboard	0.013	0.25	825	1008
Clay brick	0.3	1.1	960	2000
Insulation	0.10	0.032	29	840
Plasterboard	0.013	0.25	825	1008
Clay brick	0.20	1.1	960	2000
Double glazing	0.024	0.09	2500	750
Wood	0.20	0.26	29	840
Tiled floor	0.02	1.2	2000	1000
Soil	2.0	1.5	1250	900

Figure 4: thermal characteristics materials

2.3.2. Convection

Indoor and outdoor convective heat exchanges are treated separately. Outdoors, convective transfer coefficients are fixed to 20 W.m^{-2}.K^{-1} for the roof, and 10 W.m^{-2}.K^{-1} for the other surfaces within the urban scene. They are a dependent of the outdoor temperature from the weather data.

Indoor, the convective transfer coefficient depends of flux direction: 2.5 W.m^{-2}.K^{-1} for horizontal flux, 0.7 W.m^{-2}.K^{-1} for ascending, and 5 W.m^{-2}.K^{-1} for descending [14]. The indoor air temperature is recalculated at each time step by using the virtual conductive node method [4]. Centred in each close space, nodes are related to five-node pyramidal elements. The convection transfer coefficient, defined as previously, is applied to each interior surface. In addition, an air renewal rate of 0.8 vol.h^{-1} is applied to model heat exchanges with the exterior, according to equation (2), with $\emptyset_v$ as the thermal flux [W/m²], V_i as the air flow renewal rate [m^3.h^{-1}], ρ_{air} the air density [kg.m^{-3}], $C_{p,air}$ as the specific heat [J.kg^{-1}.K^{-1}], and $\Delta T_{ext-int}$ as the difference between interior and exterior temperature [K].

$$\emptyset_v = \left(V_i * \rho_{air} * C_{p,air}\right) * \Delta T_{ext-int} \quad (2)$$

2.3.3. Radiation

The irradiances of the faces (shortwave and longwave) from the sky are used as boundaries conditions at each time step. In addition, a longwave radiation exchange resolution method integrated in Cast3m modified is used. The Gauss-Seidel algorithm has been replaced by the Jacobi algorithm, which approximates radiosity as being equal to emission [4]. It permits to calculate the radiation between all faces at each time step from the previously calculated view factors.

In this study, the radiation exchanges between the three different cases are illustrated above (**figure 3***)*. The longwave view factors used for the first case are calculated the real environment of the street, and the second and the third one used the view factors calculated as an open field.

2.4. Comfort model

The comfort assessment uses physiological equivalent temperature (PET) indicator [15]. It corresponds to the air temperature in a typical indoor environment where the human body's thermal equilibrium is maintained (light activity of 80 W, thermal resistance of clothing of 0.9 clo). This indicator, commonly used for outdoor comfort, integrates the full radiant spectrum (shortwave and longwave) and has been recently used to assess the risk of indoor overheating [16].

To model the radiation received by the sensors, a black globe with a diameter of 0.15 meters is divided into 50 oriented surfaces [17] that see their environment but are not seen **(figure 5)** and receive the radiation without interacting, emitting, reflecting, transmitting or absorbing it, so they have no influence on its distribution. The shortwave radiation is calculated from the sky before the finite element calculation, and the longwave radiation is calculated after the finite element calculation regarding the surface temperature of the scene and the longwave view factor of the sensors.

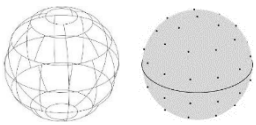

Figure 5: Representation of a black globe. Left: decomposition into 50 surfaces with equivalent solid angles. Right: representations of the 50 "sensor" points at the centre of each face.

Total radiation received for both shortwave and longwave is converted to mean radiant temperature according to using equation (3). T_{mr} is the mean radiant temperature [K], $\emptyset_r$ is the radiant flux received by the sensor [W], σ is the Stefan-Boltzmann constant [W.m^{-2}.K^{-1}], $\varepsilon_{g,lw}$ is the emissivity of the black globe, considered as a black body ($\varepsilon_{g,lw} = 1$).

$$T_{mr} = \sqrt[4]{\frac{\emptyset_r}{\sigma * \varepsilon_{g,lw}}} \tag{3}$$

The mean radiant temperature is then integrated into equations (4) and (5) used to calculate the PET [K], regarding S_{skin} S_{clo} as respectively the thermal stress due to skin and clothing radiation [W.m^{-2}.K^{-1}], $A_{r,eff}$ as the effective radiant exchange area [m²], $f_{a,cl}$ as the clothing factor, ε_{skin} ε_{clo} as the emissivity of the skin and clothing, T_{skin} T_{clo} are skin and clothing temperature [K] , and A_{dubois} as subject area [m²].

$$S_{skin} = \frac{A_{r,eff}(1-f_{a,cl})\varepsilon_{skin}\sigma(T_{mr}{}^4 - T_{skin}{}^4)}{A_{dubois}} \qquad S_{clo} = \frac{f_{eff}\ a_{clo}\ \varepsilon_{clo}\ \sigma(T_{mr}{}^4 - T_{clo}{}^4)}{A_{dubois}} \tag{4) (5}$$

In this case study, only the interior air temperature and the radiation received by the sensors are considered as variables for the PET calculation.

3. Results: indoor comfort

The equivalent physiological temperature is calculated during a heat wave for each simulation. **Figure 6** represents the mean PET of three flats calculated for each of the three variants, in relation to outdoor temperature, during a heatwave of magnitude 6, from 4th to 14th June and followed by a clear cooling over several days. In addition, the PET difference between each flat (R+0, R+1, R+2) is represented regarding the influence of longwave radiative trapping (case 2 – case 1) and shortwave inter-reflections (case 3 – case 2).

To initialize the calculation, the first case is first run during 7 days of stabilization from May 26th to June 2nd. The nodes temperatures calculated at the end of this period are used as initial conditions for further calculation of the 3 cases.

It appears that the second case has a lower PET of around 4°C than the first case for R+1/ R+2 flats and around 3.5°C for the R+0 flat, due to the increase in passive cooling by long-wave radiation.

The third case, which doesn't take account of shortwave interreflections shows variations between ±1°C which seems to follow the temperature difference with the outside, and solar radiation.

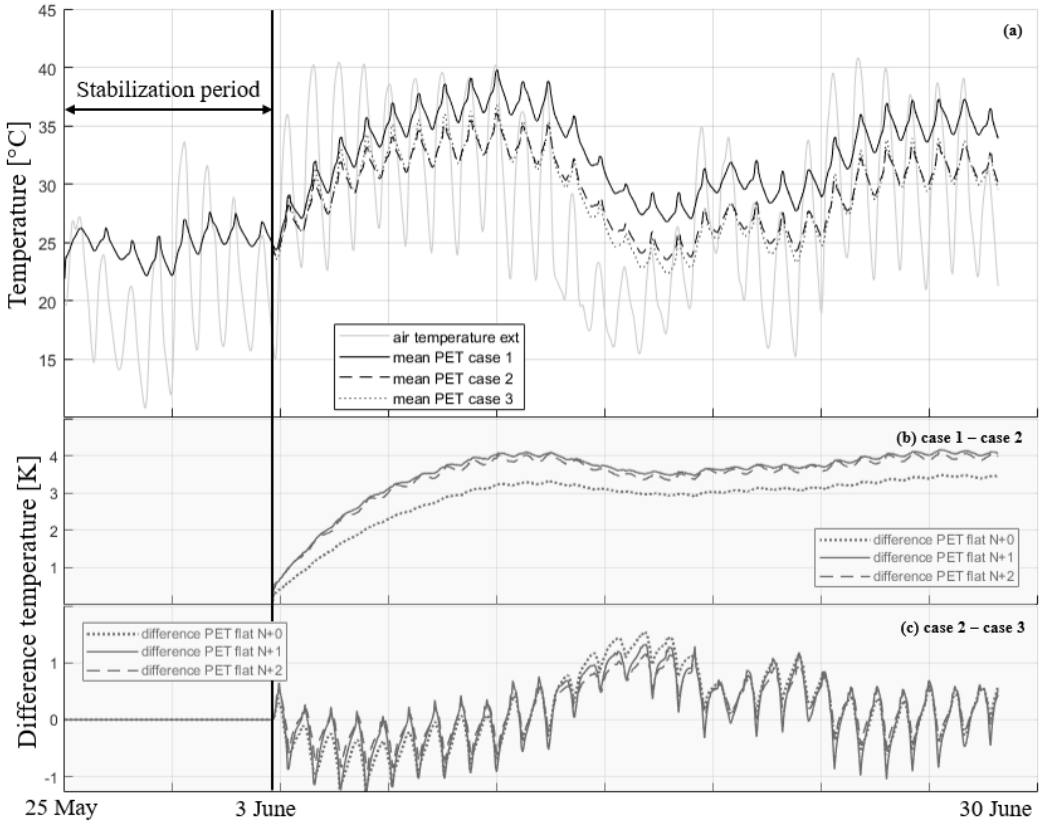

Figure 6: temperature of the three simulations, from top to the bottom: (a) mean PET of the 3 flats for each case
(b) difference of PET between case 1 and case 2 for each flat (longwave radiative trapping)
(c) difference of PET between case 2 and case 3 for each flat (shortwave radiative trapping)

4. Conclusion

The proposed work involves a numerical finite element model coupled with a radiosity method developed for the study of urban radiation to simulate the indoor thermal environment of urban buildings during heatwave. We demonstrate that in our study, the contribution of long-wave radiative trapping leads to an approximate 4 °C increase in the equivalent physiological temperature experienced by occupants within dwellings. By contrast, the influence of short-wave interreflections leads to a variable temperature difference between ±1°C. Further analyses to analyze energy flows are needed to precisely identify the reason.

This paper proposes a pathway to improve Urban Building Energy Models (UBEM) by coupling finite element simulations with a high-fidelity radiosity method applied on a detailed mesh. Moreover, this approach enables the generation of finely resolved outdoor temperature fields, comparable to urban thermography data, thereby opening opportunities for validating UBEM at higher spatial resolutions.

Although no experimental validation is currently available, a measurement campaign using black globe thermometers, thermocouples, and urban thermography is planned to verify the boundary and initial conditions of the model, and to ensure that the simulated radiative environment and indoor temperature fields faithfully represent real conditions.

Acknowledgements

This work was supported by and the "Institut Carnot – MECD" and project "ISCORT – **I**mpact **s**ur le **co**nfort d'été de la **r**enovation **t**hermique de différents typologies de logements en milieu urbain".

References

[1] M. Smid, S. Russo, A. C. Costa, C. Granell, and E. Pebesma, 'Ranking European capitals by exposure to heat waves and cold waves', *Urban Clim.*, vol. 27, pp. 388–402, Mar. 2019, doi: 10.1016/j.uclim.2018.12.010.

[2] T.R. Oke, 'The energetic basis of the urban heat island', 1982, doi: https://doi.org/10.1002/qj.49710845502.

[3] R. D. Morales, A. Audenaert, and S. Verbeke, 'Thermal comfort and indoor overheating risks of urban building stock - A review of modelling methods and future climate challenges', *Build. Environ.*, vol. 269, p. 112363, Feb. 2025, doi: 10.1016/j.buildenv.2024.112363.

[4] N. Duport, 'Études thermiques urbaines à différentes échelles par éléments finis', phdthesis, Université de Pau et des Pays de l'Adour, 2021. Accessed: Nov. 16, 2023. [Online]. Available: https://theses.hal.science/tel-03520505

[5] E. Garcia-Nevado, N. Duport, A. Bugeat, and B. Beckers, 'Benefits of street sun sails to limit building cooling needs in a mediterranean city', *Build. Environ.*, vol. 187, p. 107403, Jan. 2021, doi: 10.1016/j.buildenv.2020.107403.

[6] A. Bugeat, 'Développement d'une méthode de radiosité pour l'étude du rayonnement solaire en milieu urbain', These de doctorat, Pau, 2020. Accessed: Nov. 19, 2023. [Online]. Available: https://www.theses.fr/2020PAUU3032

[7] '\climatewebsite\WMO_Region_6_Europe\FRA_France'. Accessed: Mar. 25, 2025. [Online]. Available: https://climate.onebuilding.org/WMO_Region_6_Europe/FRA_France/index.html

[8] A. Toesca, D. David, K. Johannes, and M. Lussault, 'Generation of weather data for the assessment of building performances under future heatwave conditions', *Build. Environ.*, vol. 242, p. 110491, Aug. 2023, doi: 10.1016/j.buildenv.2023.110491.

[9] B. Beckers and P. Beckers, 'A general rule for disk and hemisphere partition into equal-area cells', *Comput. Geom.*, vol. 45, no. 7, pp. 275–283, Aug. 2012, doi: 10.1016/j.comgeo.2012.01.011.

[10] R. Perez, R. Seals, and J. Michalsky, 'All-weather model for sky luminance distribution—Preliminary configuration and validation', *Sol. Energy*, vol. 50, no. 3, pp. 235–245, Mar. 1993, doi: 10.1016/0038-092X(93)90017-I.

[11] M. Martin and P. Berdahl, 'Summary of results from the spectral and angular sky radiation measurement program', *Sol. Energy*, vol. 33, no. 3, pp. 241–252, Jan. 1984, doi: 10.1016/0038-092X(84)90155-5.

[12] 'Accueil | Cast3M'. Accessed: Feb. 15, 2024. [Online]. Available: https://www-cast3m.cea.fr/index.php

[13] L. Quiroz and P. Beckers, 'Non-conforming mesh gluing in the finite elements method', *Int. J. Numer. Methods Eng.*, vol. 38, no. 13, pp. 2165–2184, 1995, doi: 10.1002/nme.1620381303.

[14] CSTB, 'CSTB (Centre Scientifique et Technique du Bâtiment), Règles Th-U Fascicule 4: Parois Opaques, CSTB Editions, 2012.' 2012.

[15] P. Höppe, 'The physiological equivalent temperature - a universal index for the biometeorological assessment of the thermal environment', *Int. J. Biometeorol.*, vol. 43, no. 2, pp. 71–75, Oct. 1999, doi: 10.1007/s004840050118.

[16] S. Attia *et al.*, 'Overheating calculation methods, criteria, and indicators in European regulation for residential buildings', *Energy Build.*, vol. 292, p. 113170, Aug. 2023, doi: 10.1016/j.enbuild.2023.113170.

[17] B. Beckers and P. Beckers, 'Complete set of Matlab procedures for achieving uniform ray generation', 2016.